# Novel Sn-based photoresist for high aspect ratio patterning

Mengjun Li, Viacheslav Manichev, Fangzhou Yu, Danielle Hutchison, May Nyman, et al.

Mengjun Li, Viacheslav Manichev, Fangzhou Yu, Danielle Hutchison, May Nyman, Torgny Gustafsson, Leonard C. Feldman, Eric L. Garfunkel, "Novel Sn-based photoresist for high aspect ratio patterning," Proc. SPIE 10586, Advances in Patterning Materials and Processes XXXV, 105860K (13 March 2018); doi: 10.1117/12.2297440

SPIE.

Event: SPIE Advanced Lithography, 2018, San Jose, California, United States

# Novel Sn-Based Photoresist for High Aspect Ratio Patterning

Mengjun Li*[a], Viacheslav Manichev[a], Fangzhou Yu[c], Danielle Hutchison[e], May Nyman[e], Torgny Gustafsson[b, d], Leonard C. Feldman[b, d], Eric L. Garfunkel[a, b, d]
[a]Department of Chemistry and Chemical Biology, [b]Department of Physics and Astronomy,
[c]Department of Electrical and Computer Engineering and [d]Rutgers Institute for Advanced Materials, Devices and Nanotechnology,
Rutgers University, 610 Taylor Rd, Piscataway, NJ 08854 USA
[e]Department of Chemistry, Oregon State University, Corvallis, OR 97331

## ABSTRACT

Extreme ultraviolet (EUV) lithography is expected to replace current photolithographic methods because of improved resolution. The atomic photon absorption cross section is a central factor that determines the optimal elements around which to base photoresist chemistry, and tin is a strong absorber for EUV photons (~92 eV). β-$NaSn_{13}$ ($[NaO_4(BuSn)_{12}(OH)_3(O)_9(OCH_3)_{12}(Sn(H_2O)_2)]$), one of the organo-tin oxo compounds is being studied in this paper using helium ion beam lithography (HIBL) to demonstrate the patterning performance. High aspect ratio (15:1) and dense line patterns (20 nm half pitch) have been achieved with no defects. Thinner films yielded even smaller feature sizes (linewidths of ~ 10 nm). Thinner films require higher dose to get continuous and solid line patterns presumably due to fewer molecules available for condensation. Studies on various substrates indicate that the high Z substrates can help improve the pattern performance at low doses.

**Keywords:** β-$NaSn_{13}$, HIML, High aspect ratio, substrate dependence, thickness dependence, Monte Carlo simulation, secondary electrons

## 1. INTRODUCTION

Materials with high aspect ratio features have very broad and significant applications including FinFETs, diffractive optics, battery anodes and sensors [1]-[2][3]. The lithography step is the heart of the process. Especially for transistors, dense critical three dimension patterns are required in a Moore's law scenario for low cost and high performance. After decades of efforts by industrial and academic researchers, EUVL will soon been applied in high-volume manufacturing semiconductor processing [1]. Some issues of the EUVL hardware are still to be solved like inadequate source power, pellicles and defects from the masks. Nevertheless, the material for the photoresist for EUVL becomes a major focus for material scientists. The proper material requires optimization of several basic parameters: sensitivity, critical dimension and the etching selectivity. Metal-based photoresists usually have better resistivity to either wet or dry etching. Also the EUV absorption cross sections of metals are higher than that of carbon or oxygen in organic resists. Hafnium, antimony and tin are three popular metals with high absorption cross sections that have been studied as photoresist metal core [5][6]. In this paper we report the use of Helium Ion Beam Lithography (HIBL) to prescreen EUV resists prior to the evaluation in the EUV scanner. Helium ions scatter less than electrons, and produce fewer energetic recoil-atoms as compared to heavy ion irradiation. The negligible proximity effect of HIBL also helps give very high lateral resolution [7]. A comparison between EUV and 30 keV helium ion exposure was reported earlier showing highly similar trends in dose response. One single 30 keV helium ion can be as effective as 150 EUV photons in terms of secondary electron generation. Hence the HIBL has important advantages for critical dimension patterning and serves as a stringent test of resist performance [8].

In order to get critical dimension features without pattern collapse and other detrimental issues, thinner films around 20 nm or even less are required [8]. With thin films, the energy and secondary electrons from the substrates induced by the incident ion, electron or photon beam might also play a role in the lithography process, a secondary process that has only been studied to a limited extent. One simulation of EUV exposures shows a significant difference between copper and silicon substrates [8], related to higher absorbed energy in copper based materials causing additional chemistry interactions.

Advances in Patterning Materials and Processes XXXV, edited by Christoph K. Hohle, Proc. of SPIE
Vol. 10586, 105860K · © 2018 SPIE · CCC code: 0277-786X/18/$18 · doi: 10.1117/12.2297440

β-$NaSn_{13}$ resist with oxo-hydroxo bonds was first reported to show potential for radiation-induced condensation for photoresist applications [11]. We now describe below the patterning properties of β-$NaSn_{13}$ resist combined with etching resistance tests using HIBL. Monte Carlo simulations were also performed to explain the thickness and substrate dependence in the lithography.

## 2. EXPERIMENTAL DETAILS

**The preparation of the β-$NaSn_{13}$ precursor solution** $[NaO_4(BuSn)_{12}(OH)_3(O)_9(OCH_3)_{12}(Sn(H_2O)_2)]$ followed a slightly modified literature procedure [11]. BuSnOOH (Sigma-Aldrich) was suspended in methanol (Sigma-Aldrich) at a concentration of 0.08 g/mL. The solution was sonicated to ensure maximum dissolution of soluble material, and then centrifuged to remove insoluble material. The supernatant was transferred to a closed glass container and allowed to sit undisturbed at room temperature. Within one day, crystals would grow and were isolated from the walls of the container. The supernatant was removed under reduced pressure to collect solid precursor crystals. Precursor solutions were prepared in two ways to provide films with different thickness. For thicker films 20 mg/mL β-$NaSn_{13}$ solution with 2-heptanone was used as the solvent, while for thinner films the concentration was 5 mg β-$NaSn_{13}$ per 1.5 mL toluene. The films were sonicated for 5 min for complete dissolution. All samples were made fresh prior to film deposition.

**Film deposition** Three types of substrates were: single-side polished n-type As-doped Si (100) wafers (Resistance 0.001-0.005 ohm-cm) with native oxides, single-side polished p-type As-doped Si<100> wafers (Resistance 1-10 ohm-cm) with 300 nm thermal oxides and metal coated glass slides (with 10 nm gold and a ~20 angstroms titanium adhesion layer used to bind the gold to the alumina silicate glass microscope slide). Prior to the β-$NaSn_{13}$ deposition, the Si wafers were cleaned by consecutive sonication in acetone, isopropanol and deionized water (18.2 MΩ). Next, the non-oxidized Si wafers (with native oxides) were treated with 49% HF solution to create a hydrogen terminated surface without oxides. The precursor solutions were filtered by 0.45 μm PTFE (Polytetrafluoroethylene) filters and then deposited by spin coating (Laurell Technologies) at 3000 rpm for 30 s with an acceleration rate of 3000 rpm/s, and finally soft baked at 70 °C for 3 mins. For thinner film, HMDS (hexamethyldisilizane) was used to enhance adhesion of the photoresist to the surfaces by spin dry with 3000 rpm for 30 s. After cooling in air, the films were ready for patterning and characterization.

**Characterization:** Films were characterized by atomic force microscopy (AFM) using Park Systems NX-10 with z-scan noise level of about 0.2 Å. Measurements were done in the non-contact mode with a PPP-NCHR tip (Nanosensors, tip radius <10 nm). Rutherford backscattering spectrometry (RBS) was performed using a 2MeV $He^+$ beam from a 1.7 MV tandem accelerator with an ion current of 2-3 nA. Data fitting and modeling were accomplished using the SIMNRA 6.06 software package.

**Helium ion beam lithography and microscopy** A Carl Zeiss ORION PLUS HIM system was used for patterning and imaging. The Orion produces a 30KeV $He^+$ beam with beam spot sizes as small as 0.5 nm. The lithography current was kept below 1 pA. Pixel spacing was 1 nm. The nominal line width was set by the software ranging from 1 nm to 20 nm in order to determine the best critical dimensions under given lithography conditions. Following the helium ion exposure, a post exposure bake was applied at 175 °C for 5 mins. Then the films were developed in 2-heptanone for 1 min and blow dried with compressed nitrogen.

**Etching Setup** With β-$NaSn_{13}$ as photoresist, silicon was etched anisotropically using Oxford Plasmalab 100 inductively coupled plasma (ICP) etcher in 15 mTorr $O_2/SF_6$ plasma with a flow rate 15 sccm/40 sccm, respectively. The cryogenic process was maintained at -100 °C with 15 W of RF power for 10 s. High aspect ratio walls were etched in silicon to a depth of 300 nm at an etch rate 30 nm/s.

**Pattern analysis** The line edge roughness (LER) and critical dimension (CD) were calculated from high-resolution, top-down secondary electron images of sets of three patterned lines acquired using the Scanning Helium Ion Microscope (SHIM) and following the methods recommended by the ITRS [12]. Images were processed using the image processing software ImageJ. The images were smoothed and adjusted to better contrast for convenient determination of the line edges. Each line was extracted with boxes that include its edges completely. A histogram profile was generated for choosing edges to calculate the average width, width standard deviation, and edge position standard deviation. LER was

calculated as three times the standard deviation in the line edge position (average from top and bottom line edges), and the CD is the line width.

**Monte Carlo simulation** The commercial software SRIM package (the stopping and range of ions in matter) was used to simulate the trajectories of the helium ions. The film composition was set as the cluster and film density determined by RBS. Simulations were performed with one thousand 30 keV He ions .

## 3. HIGH ASPECT RATIO DENSE LINE PATTERNS

### 3.1 Dose optimization for dense line patterns

We used 20 nm thick films to investigate the etching selectivity and pattern stability of the resist. An array of 2×2 $\mu m^2$ square patterns was made by the 30 keV helium ion beam with different doses. AFM measured the remaining film thickness yielding the β-$NaSn_{13}$ resist contrast curve in Figure 1(a). $D_{100}$ (the dose at which the developed features start to have 100% of the as-deposit resist thickness) is about 11 $\mu C/cm^2$, comparable to the sensitivity of modern (organic) photoresists [13]. However higher dose was required to make the straight and solid lines shown in Figure 1(b). With a dose of 10 $\mu C/cm^2$, we observed discontinuities and wiggles while with a dose of 20 $\mu C/cm^2$, photoresist bridging occurred. Only a dose of 15 $\mu C/cm^2$ gives us line patterns without defects. The difference in doses needed for making square and line patterns shows that lateral crosslinking may enhance the sensitivity of the resist. Choosing the proper dose for various kinds of patterns might help optimize processing time as well as patterning performance. 20 nm half pitch dense line patterns were achieved after optimization.

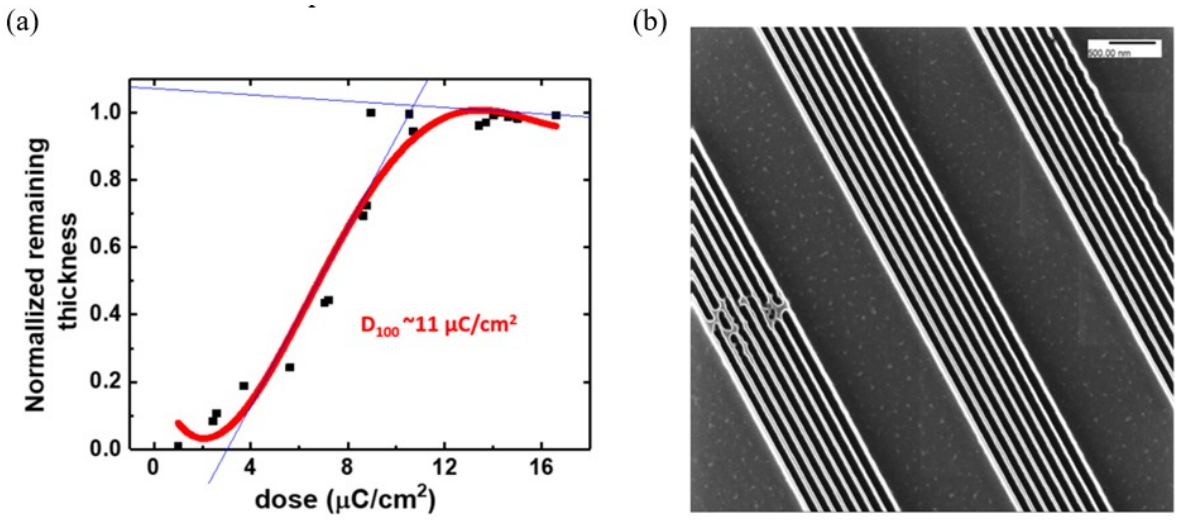


Figure 1. (a) The contrast curve of β-$NaSn_{13}$ resist with 30 keV HIBL, and (b) HIM image of dense line patterns exposed with three doses, 20, 15, 10 $\mu C/cm^2$ individually from left to right. Scale bar: 500 nm.

### 3.2 High aspect ratio patterning

To check the etching resistance of β-$NaSn_{13}$ for maintaining a high aspect ratio, an $O_2/SF_6$ inductively coupled plasma was used on both square and line patterns. The square corner in Figure 2(a) presents very sharp edges. The AFM line profile in Figure 2(b) exhibits an etched pattern height of around 300 nm. Figure 2(c) and (d) show top-down and side views (40° angle) of 20 nm wide and 300 nm tall line patterns using SHIM imaging. This gives us the aspect ratio of 15:1. Although the side wall was roughened due to the etching process, there is no bridging or other defect. The silicon beneath the resist mask was etched laterally to a small extent which would give even narrower trenches after removal of

the resists. About 80% of the resist width was maintained with this anisotropic etching, higher aspect ratios with smaller feature sizes should be possible with further etching.

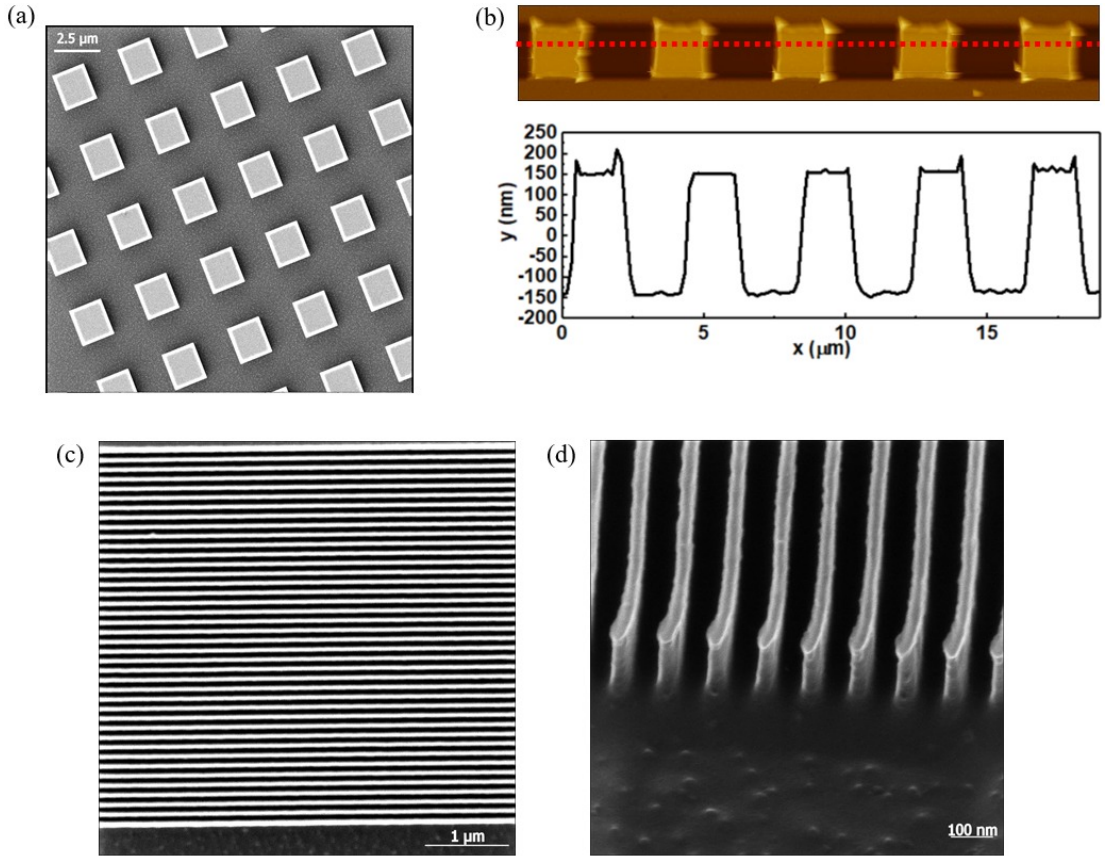


Figure 2. (a) SHIM image of etched square patterns with scale bar of 2.5 µm. (b) AFM line profile of etched square patterns. (c) Top-down view and (d) 40° tilted angle images of etched dense line patterns.

## 4. THICKNESS AND SUBSTRATE DEPENDENCE

### 4.1 Thickness dependence

We studied 10 nm thick films to investigate the critical dimensions and sensitivity compared to 20 nm thick films. The best critical dimension patterns in Figure 3 indicate an average line width as 8.8 nm and LER of 2.1 nm with 10 nm films while with 20 nm films the best average line width was 20.2 nm with LER as 4.2 nm.

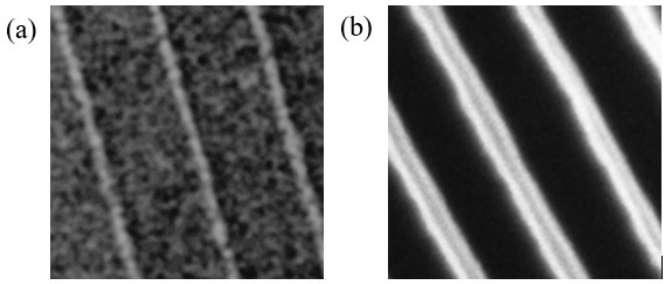


Figure 3. (a) and (b) are SHIM images of line patterns used to calculate CD and LER for 10 nm and 20 nm thick film individually.

Similar optimization of other doses for line patterns were performed and the HIM images are shown in Figure 4. With 10 μC/cm$^2$, lines with nominal width less than 5 nm can be barely seen, while using 20 μC/cm$^2$ those lines are solid and continuous. Based on previous study [11], the cluster radius is about 5 Å according to both simulation and scattering data. 15 μC/cm$^2$ corresponds to just about 1 ion/nm$^2$.

The incident ion energy loss per Ångström due to ionization should be independent of the resist thickness. In thicker line patterns, one ion per resist cluster may be enough to trigger and complete the condensation chemistry. In thinner films, the total amount of clusters in the vertical direction is at most half of that for thicker films. As the ion penetrates the resist film, it might miss some clusters and transfer insufficient energy to the cluster. As a result, fewer secondary electrons might be generated and the number of polymerized clusters will not be enough for maintaining pattern shape and continuity.

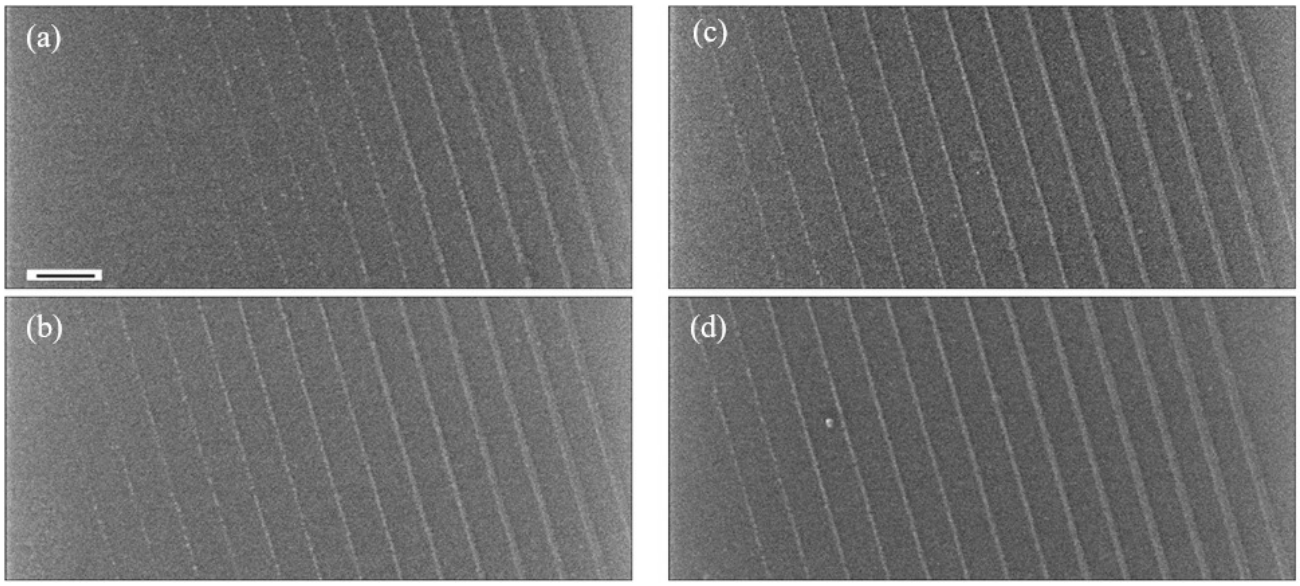


Figure 4. (a), (b), (c) and (d) HIM images of line patterns exposed with doses of respectively 10, 15, 20, and 25 μC/cm$^2$. The scale bar is 200 nm for all images. The nominal line widths are 1, 2, 3, 4, 5, 10, 15, and 20 nm from left to right. A pair of each lines are shown.

### 4.2 Substrate dependence

We applied 10 nm films with HMDS as the adhesion layer on Si, $SiO_2$ and Au individually. A set of line patterns with dose of 15 μC/cm$^2$ were made on these three samples. The resulting AFM and HIM images are shown in Figure 5. Two lines with 1 nm as the nominal width were almost invisible. Eight lines with 2, 3, 4, 5 nm as the nominal width were used to compare the patterning limitation at a given dose. Based on the AFM images and their line profiles, the heights of lines of interest on Si and Au substrates are around 5 nm, comparable to wider lines that have been fully exposed. As to the lines on $SiO_2$ substrate, the heights of lines with 2 and 3 nm nominal width are less than 3 nm. So its condensation is not complete and it might not be able to serve as a good mask in manufacturing. In addition, the lines on Si with 2 and 3 nm nominal width are not as continuous as lines on Au which may also introduce defects in the Si case. Only the lines on Au are solid straight with good continuity. This result indicates that the substrates can actually play an important role in manipulating patterning properties.

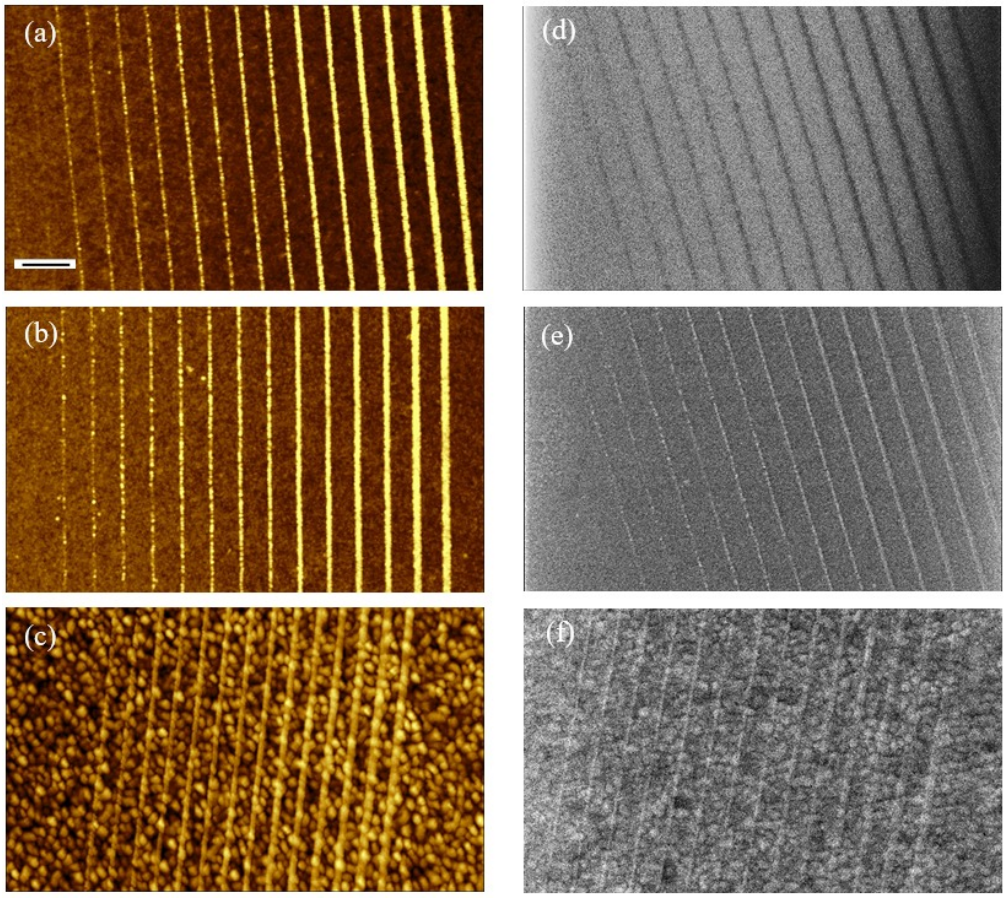


Figure 5. AFM images (a), (b) and (c), HIM images and (d), (e) and (f) of line patterns exposed to 15 μC/cm$^2$ on $SiO_2$, Si and Au coated glass substrate. The scale bar is 200 nm for all images. The nominal line widths are 1, 2, 3, 4, 5, 10, 15, and 20 nm from left to right. A pair of each lines are shown.

In this case, we are interested in particles (secondary electrons) emitted from the substrate surface which may have sufficient energy to trigger resist condensation. Thus the secondary electron yield from the substrate may affect the lithography. There are studies using Monte Carlo simulations to calculate the ion induced secondary electron yield that can escape from the surface. The simulation results using 40 keV helium ions by Huh, were quite similar to our experimental conditions [15]. One sees that Au has about 8 times of secondary electron yield compared to Si. This could enhance the sensitivity of the resist significantly if such secondary electrons can transfer energy and induce chemical changes to the film.

We also explored the trajectories of helium ions and ionizations in three samples simulated using TRIM software. The trajectories, shown in Figure 6(a) for the three substrates, indicate similar lateral dimension and total amount of ionization in the resist films. The only difference concerns the 10-20 nm region where gold generates more ion backscattering and therefore more energy deposition in the gold layer. The energy loss as a function of target depth is plotted in Figure 6(b). With similar energy loss in the photoresist, the ionization in the three substrates shows huge differences. $SiO_2$ has even smaller ionization efficiency than the resist film itself. On the contrary, Au shows more than twice the electronic energy loss than the resist. Much more energy was deposited within the 20 nm depth range.

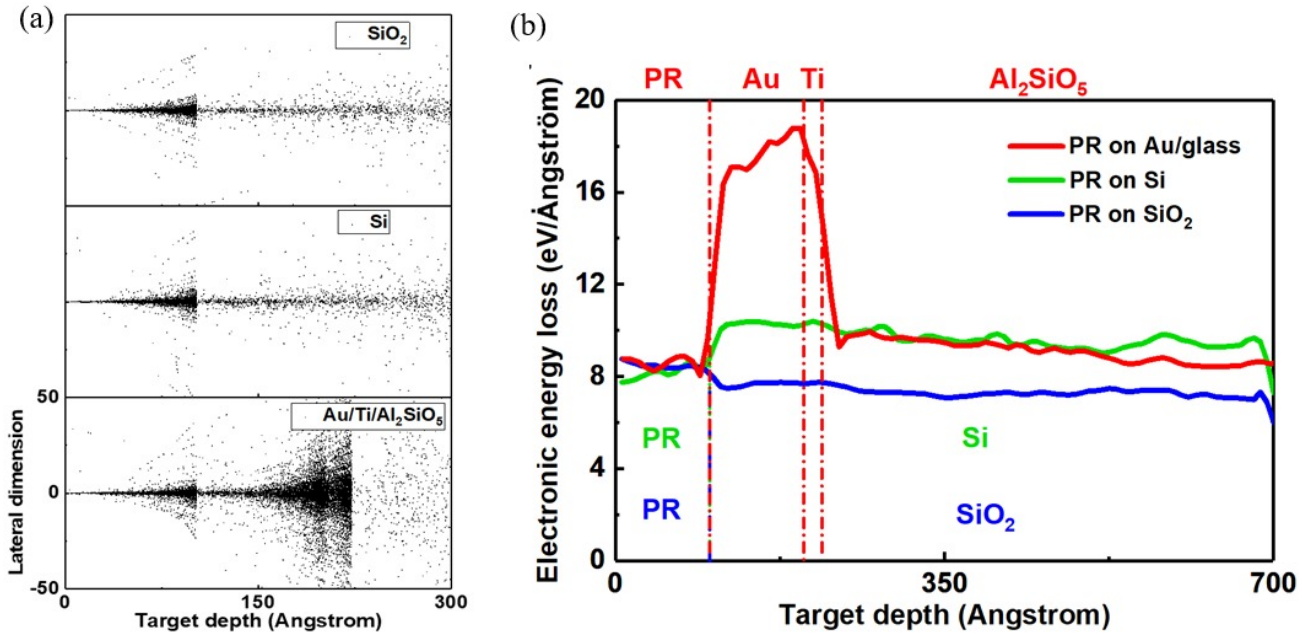


Figure 6. Monte Carlo simulation of (a) ion trajectories and (b) energy loss due to ionization in three samples with β-$NaSn_{13}$ photoresist (PR) on gold coated glass, silicon and silicon oxide substrates.

## 5. CONCLUSIONS

We have investigated the β-$NaSn_{13}$ resist patterning performance using HIBL. Both sensitivity and etching selectivity were satisfactory. High aspect ratio structures (15:1) with dense line patterns (20 nm half pitch) were made under optimized exposure flux and etching condition. Our experimental results and Monte Carlo simulation studies show that thinner resist films can give smaller feature sizes while substrates with higher secondary electron yield can give improved resist sensitivity. With such optimized conditions better lithography efficiency and pattern properties can be achieved.

## ACKNOWLEDGEMENTS

The authors gratefully acknowledge the support of the National Science Foundation via the Center for Sustainable Materials Chemistry (an NSF-Center for Chemical Innovation), under Grant CHE-1606982.

## REFERENCES

[1] Morton, K. J., Nieberg, G., Bai, S. and Chou, S. Y., "Wafer-scale patterning of sub-40 nm diameter and high aspect ratio (> 50: 1) silicon pillar arrays by nanoimprint and etching," Nanotechnology 19(34), p.345301 (2008)

[2] Aguilar-Morales, A. I., Alamri, S. and Lasagni, A. F., "Micro-fabrication of high aspect ratio periodic structures on stainless steel by picosecond direct laser interference patterning," Journal of Materials Processing Technology 252, pp.313-321 (2018)

[3] Ozel, T., Zhang, B. A., Gao, R., et al., "Electrochemical Deposition of Conformal and Functional Layers on High Aspect Ratio Silicon Micro/Nanowires," Nano letters 17(7), pp.4502-4507 (2017)

[4] Moore, K. S., "EUV Lithography Finally Ready for Chip Manufacturing," IEEE spectrum, 5 Jan 2018, https://spectrum.ieee.org/semiconductors/nanotechnology/euv-lithography-finally-ready-for-chip-manufacturing, (2018)
[5] Oleksak, R. P., Ruther, R. E., Luo, F. X. et al., "Chemical and Structural Investigation of High-Resolution Patterning with HafSOx," ACS Applied Materials & Interfaces 6(4), 2917-2921 (2014).
[6] Li, L., Liu, X., Pal, S., Wang, S., Ober, C.K. and Giannelis, E. P., "Extreme ultraviolet resist materials for sub-7 nm patterning," Chemical Society Reviews 46(16), pp.4855-4866 (2017)
[7] Luo, F., Manichev, V., Li, M. et al., "Helium ion beam lithography (HIBL) using HafSOx as the resist," Advances in Patterning Materials and Processes XXXIII 9779, p. 977928 (2016)
[8] Maas, D., van Veldhoven, E., van Langen-Suurling, A. et al., " Evaluation of EUV resist performance below 20nm CD using helium ion lithography," Extreme Ultraviolet (EUV) Lithography V 9048, p. 90482Z (2014)
[9] Buitrago, E., Fallica, R., Fan, D. et al., "SnOx high-efficiency EUV interference lithography gratings towards the ultimate resolution in photolithography," Microelectronic Engineering 155, pp.44-49. (2016)
[10] Wiseheart, L., Narasimhan, A., Grzeskowiak et al., "Energy deposition and charging in EUV lithography: Monte Carlo studies," Extreme Ultraviolet (EUV) Lithography VII 9776, p. 97762O (2016)
[11] Saha, S., Park, D. H., Hutchison, D. et al., "Alkyltin Keggin Clusters Templated by Na," Angewandte Chemie International Edition (2017)
[12] ITRS, "Metrology," (2009).
[13] De Simone, D., Vanelderen, P. and Vandenberghe, G., "Photo Material Readiness at the Eve of EUVL HVM," Journal of Photopolymer Science and Technology 30(5), pp.613-617 (2017)
[14] Dapor, M., "Secondary electron emission yield calculation performed using two different Monte Carlo strategies," Nuclear Instruments and Methods in Physics Research Section B: Beam Interactions with Materials and Atoms 269(14), pp.1668-1671 (2011)
[15] Huh, U, "Monte Carlo Modeling of Ion Beam Induced Secondary Electrons," PhD dissertation., University of Tennessee, http://trace.tennessee.edu/utk_graddiss/2832 (2014)